9-6-2011

Electrowetting-Induced Dewetting Transitions on Superhydrophobic Surfaces

Niru Kumari
Birck Nanotechnology Center, Purdue University

Suresh V. Garimella
Birck Nanotechnology Center, Purdue University, sureshg@purdue.edu

Langmuir

LETTER

pubs.acs.org/Langmuir

Electrowetting-Induced Dewetting Transitions on Superhydrophobic Surfaces

Niru Kumari and Suresh V. Garimella*

School of Mechanical Engineering and Birck Nanotechnology Center, Purdue University, West Lafayette, Indiana 47907, United States

Supporting Information

ABSTRACT: We develop and demonstrate the use of electrowetting to achieve the dewetting (Wenzel-to-Cassie transition) of superhydrophobic surfaces. We effect this transition by means of an opposing flat plate and a three-electrode system; the liquid droplet is completely pulled out of its wetted Wenzel state upon the application of a suitable voltage. We also experimentally quantify the dissipative forces preventing the dewetting transition. The energy associated with these nonconservative forces is comparable to the interfacial energies.

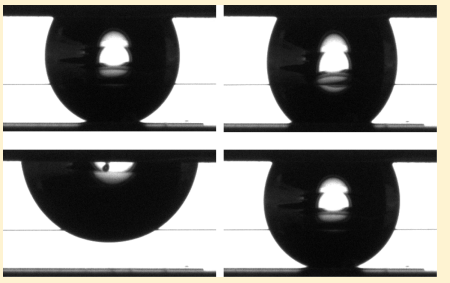

Superhydrophobicity has attracted significant attention over the past decade because of potential applications in lab-on-a-chip devices, energy systems, and heat transfer. A classical study of superhydrophobicity involves the analysis of a droplet in a Cassie state[1] (nonwetting) as depicted in Figure 1a, wherein the droplet rests only on the tips of the surface features. The other extreme of wettability is studied as a Wenzel state[2] (Figure 1b) in which the droplet wets the surface features completely. Patankar[3] showed that the Cassie and Wenzel droplets differ in their surface energies, and the stable equilibrium state of the droplet on a particular surface corresponds to the state that has the lower energy.

Electrowetting (EW)[4] has been characterized as a tool for effecting the Cassie−Wenzel transition on superhydrophobic surfaces. EW can be understood as an effective reduction in the solid−liquid interfacial energy upon the application of a voltage between a conducting droplet and an underlying dielectric layer. EW has been extensively used in various microfluidic operations such as the actuation, formation, splitting, and mixing of droplets[5−10] on smooth surfaces. EW has also been utilized to induce the Cassie−Wenzel transition on microstructured[11−13] and nanostructured[14−17] superhydrophobic surfaces. Two recent reviews[18,19] discuss various aspects of electrowetting on superhydrophobic surfaces. A key observation in such wettability studies is the lack of complete and spontaneous reversibility of the Cassie−Wenzel transition upon removal of the EW voltage.[13,14] The primary reasons inhibiting complete reversibility are the presence of an energy barrier for the reverse transition and frictional dissipative forces.[13,14] Dissipative forces opposing fluid motion in the Wenzel state include contact line pinning, contact line friction, and wall shear. These dissipative forces have not been quantified in the literature.

A few attempts at achieving the dewetting Wenzel−Cassie transition have been successful, but each suffers from some inherent disadvantages. Krupenkin et al.[14] passed a current pulse through the substrate to vaporize a layer of liquid at the substrate−liquid interface, causing the droplet to revert to a Cassie state. However, the mass loss associated with the vaporization and the added heat input are undesirable. Another method for achieving reversibility utilizes an oil environment, which promotes competitive wetting and reduces dissipative forces;[16,17] however, an oil environment is not desirable in many biological systems. The dewetting transition on natural superhydrophobic surfaces has been demonstrated using mechanical vibration;[20] this technique is also difficult to implement in lab-on-a-chip applications. Recently, the reverse transition was demonstrated on corrugated surfaces[21] but the imaging and results were inconclusive, and only corrugated surfaces with a narrow range of feature sizes were considered. Another study utilized horizontal channels with perpendicular electrodes[22] to achieve a partial Wenzel-like transition with electrowetting, reverting back to the Cassie state when the electrodes were deactivated. Lapierre et al.[23] studied the Cassie−Wenzel transition using electrowetting in ambient air on double-scaled rough surfaces (nanoscale roughness on circular microscale pillars). They noticed that the droplet reverted to the Cassie state when the applied voltage was removed for surfaces with a specific pillar height; the range of feature sizes that may be used with this approach is therefore limited. Moreover, the droplet remained in the Wenzel state after a few cycles. Lee and Kim[24] utilized electrolysis to generate a gas layer to achieve the Wenzel−Cassie transition; however, such chemical reactions may be undesirable in biological applications.

In the present work, we demonstrate that electrowetting can be used to induce the dewetting transition, in addition to the wetting transition. A three-electrode system is utilized to demonstrate that the wetting and dewetting states can be controlled using only electrical voltages. The reverse transition is reliably

Received: April 29, 2011
Published: July 19, 2011

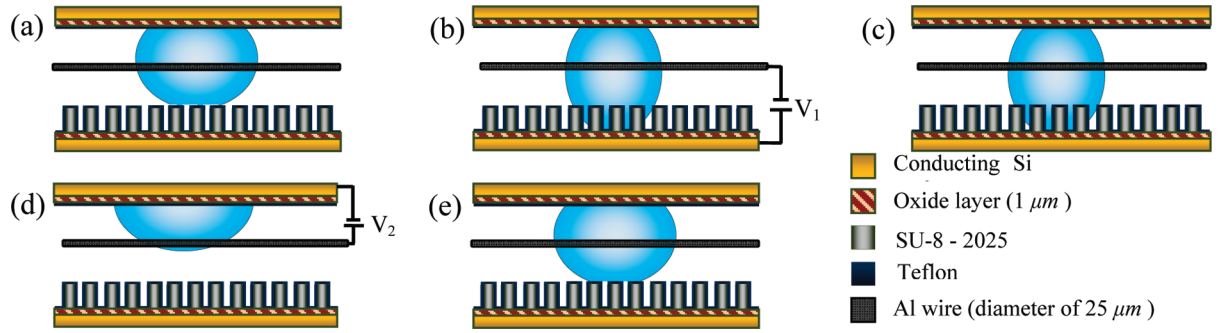

Figure 1. EW-induced wetting and dewetting transitions. (a) Initial state with a droplet in the Cassie state on a lower plate. (b) Lower plate actuation triggers the Wenzel transition. (c) The droplet persists in the Wenzel state when the lower plate voltage is turned off. (d) Dewetting transition triggered by actuation of the top plate, which causes complete droplet lift-off. (e) The droplet comes to rest on the lower plate in the Cassie state when the top plate voltage is turned off.

Table 1. Summary of Results from the Dewetting Transition Experiments

surface	pillar size a (μm), pitch b (μm), height h (μm)	φ, r_m	$h/(b-a)$	actuation voltage on bottom plate V_1 (V), EW number	critical dewetting voltage $V_{2\text{-crit}}$(V), EW number	CA on bottom plate with droplet in Cassie state (a)/(e)	CA on bottom plate with droplet in Wenzel state (b)/(c)	e_{lost} (mJ/m^2)	c_f (mJ/m^2)
1	20, 45, 22	0.2, 1.87	0.88	200, 0.16	50, 0.61	155/157	137/138	64.8	74
				250, 0.25	50, 0.61	155/156	120/133	54.0	61
				275, 0.30	65, 1.04	155/157	117/133	58.0	66
				300,0.36	65, 1.04	155/159	115/133	63.1	72
2	13, 25, 22	0.27, 2.83	1.83	275, 0.33	65, 1.04	152/154	104/124	94.4	52
3	27, 42, 22	0.41, 2.35	1.47	275, 0.39	70, 1.20	159/160	93/121	89.6	61
4	20, 45, 46	0.2, 2.82	1.84	350, 0.41	60, 0.89	165/167	120/145	106.3	58
				550, 1.01	65, 1.04	165/164	113/118	109.5	60

achieved without any liquid loss; also, no additional complexities in the surface design are introduced.

Figure 1a shows a schematic diagram of the test configuration used for inducing the wetting and dewetting transitions in a droplet using electrowetting. The droplet is sandwiched between two flat plates; additionally, a thin wire runs through the droplet as shown. The top and bottom plates and the wire form three independently addressed electrodes. The wire serves as the ground electrode, and either the top or the bottom plate can be used to apply a voltage difference between the corresponding electrode and the droplet, thereby actuating the droplet to change its morphology. The top and bottom plates are made of highly doped silicon wafers (with a resistivity of approximately 10 Ω cm) covered with a 1 μm thermally grown oxide layer. These low-electrical-conductivity wafers are used as electrodes, with the oxide layer providing insulation from the electrically conducting droplet. The bottom plate is rendered superhydrophobic by patterning square SU-8 pillars using standard lithography processes; these pillars are then coated with a thin layer of Teflon. The top plate is smooth and is covered with a thin layer of Teflon for hydrophobicity.

Four superhydrophobic surfaces of varying pillar size, pitch, and height are utilized in the present experiments (as detailed in Table 1). The table also lists values of φ and r_m, dimensionless parameters commonly used to characterize rough surfaces; φ is the ratio of the area of the tops of the pillars to the total base area, and r_m is the ratio of the total surface area (including the pillar sidewalls) to the total base area. Figure 2 shows scanning electron microscopy (SEM) images of two surfaces consisting of SU-8 pillars with $\varphi = 0.2$ and pillar heights of $H = 22$ and 46 μm. All of the surfaces were designed such that the Cassie state was lower in energy than the Wenzel state in the absence of an EW voltage.[13] Such surfaces ensure that the droplet is in the Cassie state without EW voltage and transitions to the Wenzel state when actuated; a droplet initially in the Wenzel state (without actuation) will stay in the Wenzel state (under actuation) but increases its wetted area on the superhydrophobic surfaces. The experiment to study the EW-induced wetting and dewetting transitions in a droplet is illustrated in Figure 1a–e. The droplet initially rests in a Cassie state on the superhydrophobic bottom plate and is in contact with the hydrophobic top plate as shown in Figure 1a. A voltage applied to the bottom plate (potential difference between the bottom plate and the ground wire, V_1) triggers a transition to the Wenzel state on the bottom plate (Figure 1b). The droplet stays in the Wenzel state when the voltage is turned off (Figure 1c). The reverse transition is achieved by exerting an upward force on the droplet via the application of a voltage to the top plate (potential difference between the top plate and the ground wire, V_2); at a sufficiently high voltage, the droplet overcomes the dissipative forces and lifts off the bottom plate (Figure 1d) without any residual liquid remaining on the bottom plate. The droplet is then deposited on the bottom plate by turning off the top-plate voltage; it is seen that the droplet rests on the bottom plate in the superhydrophobic Cassie state (Figure 1e), returning to its initial state as in Figure 1a. The basis for this dewetting transition is the use of a sufficiently strong opposing electric field to pull the droplet out of its Wenzel state.

dx.doi.org/10.1021/la2027412 |*Langmuir* 2011, 27, 10342–10346

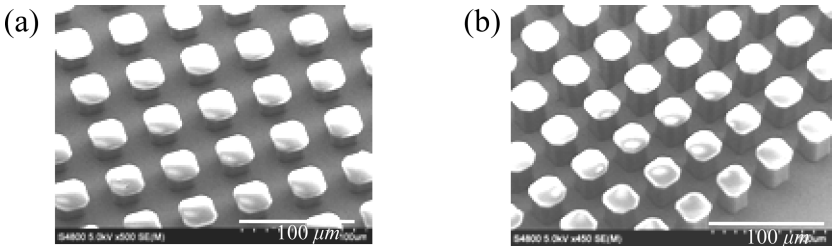

Figure 2. SEM images showing SU-8 pillars on a silicon substrate: (a) surface 1 and (b) surface 4.

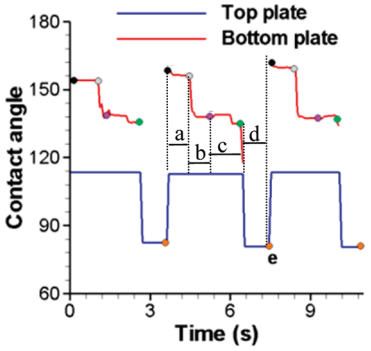

Figure 3. Time variation of the contact angle of a droplet over three wetting−dewetting cycles.

The distance between the plates determines the minimum droplet volume that can be dewetted using this approach as detailed in the Supporting Information.[25] The plate spacing in our experiments was fixed at 1.8 mm, corresponding to a minimum droplet volume of 7 μL; 7.5 μL water droplets were used in all of the experiments discussed here. Each experiment was repeated three times; the values reported below are the mean values from three separate experiments. We demonstrate the feasibility and reliability of our dewetting approach by conducting experiments that show continually repeated wetting−dewetting transitions using the same droplet. (See ref 25 for the movie.) A representative set of results is shown in Figure 3 as the time variation of the contact angle of the droplet on the top and bottom plates. The five points marked a−e on the plot correspond to the specific states of the droplet described in Figure 1. Figure 4 shows images of the corresponding droplet shapes for the first wetting−dewetting transition in a side view. The droplet is deposited on the bottom plate in a Cassie state (Figure 4a), and an EW voltage of 200 V on the bottom plate triggers the Wenzel transition (Figure 4b). The droplet retains its Wenzel state when the actuation voltage is removed (Figure 4c). The reverse transition is achieved by applying 70 V to the top plate, which lifts the droplet from the bottom plate (Figure 4d). It is noted that the time taken for this transition (not measured experimentally because of limits on the camera shutter speed) is dominated by the hydrodynamic time constant (dependent on the droplet material properties) of the droplet because the electric force time constant is much smaller in comparison. Turning off the top plate voltage causes the droplet to deposit gently onto the superhydrophobic bottom plate in the Cassie state (Figure 4e). No measurable change in the droplet volume was observed at the end of the experiment, confirming the complete reversibility of the transition without any mass loss. We note that for the timescales in this experiment, mass loss due to evaporation is negligible.

We conducted additional experiments to quantify the minimum (critical) voltage $V_{2\text{-crit}}$ on the top plate (in state d as shown in Figure 1d) necessary to lift the droplet off the bottom plate. Table 1 shows the results for all four surfaces in which we induced a droplet into the Wenzel state by applying an actuation voltage V_1 to the bottom plate. Next, for each of these wetting voltages, we increased the actuation voltage on the top plate in steps of 5 V starting from 20 V until the droplet was seen to lift off. (See ref 25 for the droplet shapes from a representative experiment on surface 2.) Table 1 lists the nondimensional electrowetting (EW) number corresponding to these voltages; the EW number is defined as the ratio of the electrical forces to the surface tension forces

$$EWnumber, \eta = \frac{k\varepsilon_0 V^2}{2d\gamma_{la}} \quad (1)$$

where k is the dielectric constant, ε_o is the permittivity of vacuum, d is the thickness of the dielectric layer, and γ_{la} is the interfacial energy of the liquid−air interface. Table 1 also lists the contact angle on the bottom plate in all of the states. We were able to lift off the droplet with voltages in the range of 50−70 V.

The measured electrical voltages and droplet shapes can be used to estimate the frictional forces in the Wenzel state. We use energy conservation arguments to estimate the amount of energy lost in the process of extracting the droplet from the Wenzel state; this lost energy is a measure of the frictional forces. The difference in the energy content of the system between state d-crit (corresponding to the critical dewetting voltage) and state c in Figure 1 is a measure of the energy lost to frictional forces:

$$E_c - E_{d\text{-crit}} = E_{lost} \quad (2)$$

The system under consideration consists of the droplet as well as the power supply providing the actuation voltages. The energy content at state d-crit (after the droplet is extracted) is estimated as

$$E_{d\text{-crit}} = E_{PS} + E_{diel} + (A_{sl}\gamma_{sl} + (A_s - A_{sl})\gamma_{sa} + A_{la}\gamma_{la})_{d\text{-crit}} \quad (3)$$

where A_{sl} is solid−liquid contact area, A_{la} is liquid−air interface area, A_s is combined solid−liquid and solid−air interfacial area in the system, and γ is the interfacial energy with subscripts sl, la, and sa denoting the solid−liquid, liquid−air, and solid−air interfaces, respectively. $E_{PS} = -CV_{2\text{-crit}}^2$ is the work done by the power supply, $E_{diel} = 0.5CV_{2\text{-crit}}^2$ is the energy stored in the capacitive layer on the top plate, and $C = k\varepsilon_o(\pi R_{top}^2)_{d\text{-crit}}\, d^{-1}$ is the capacitance. In this expression, k is the dielectric constant (3.9 for silicon oxide), ε_o is the permittivity of vacuum, and d is the thickness of the dielectric layer (1 μm). The energy content of the system in state c (the Wenzel state after the removal of the

dx.doi.org/10.1021/la2027412 |Langmuir 2011, 27, 10342–10346

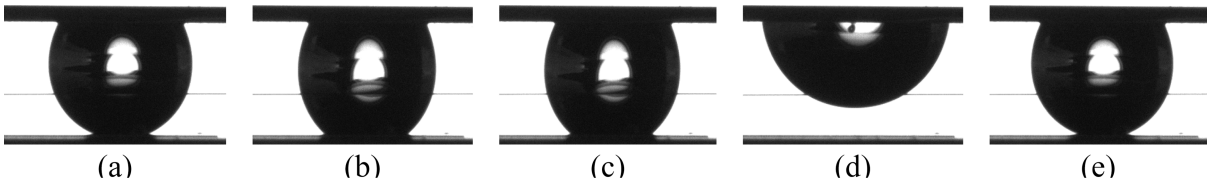

Figure 4. Visualized shapes of a water droplet corresponding to the description in Figure 1; the thin horizontal line between the top and bottom plates corresponds to the ground wire.

wetting transition voltage) is estimated as

$$E_c = (A_{sl}\gamma_{sl} + (A_s - A_{sl})\gamma_{sa} + A_{la}\gamma_{la})_c \quad (4)$$

The solid−liquid contact area includes the area on the top and bottom plates as given by $A_{sl} = \pi R_{top}^2 + r_m(\pi R_{bot}^2)$, where R is the solid−liquid interface contact radius on the top and bottom plates. Rearranging these equations, we obtain an expression for the energy lost due to frictional forces as

$$E_{lost} = \frac{1}{2}CV_{2\text{-crit}}^2 + (D_c - D_{d\text{-crit}})\gamma_{la}$$
$$where\ D = \{(\pi R_{top}^2 + r_m(\pi R_{bot}^2))\cos\theta_0 + A_{la}\} \quad (5)$$

where θ_0 is the Young's contact angle. The experimentally measured droplet profiles are used to estimate the radii and contact areas in states c and d. E_{lost} is utilized to calculate the energy lost per unit area along which liquid motion occurs during the dewetting transition (side walls of the pillars), resulting in frictional losses

$$e_{lost} = \frac{E_{lost}}{4ah \times n_{pillars}} = \frac{E_{lost}b^2}{4ah \times (\pi R_{bot}^2)_c} \quad (6)$$

where $n_{pillars}$ is the number of pillars, a is the width of the square pillar, b is the pitch between pillars, and h is the pillar height. The energy loss in the reverse transition is expected to be related to the pillar geometry. The energy losses are expected to increase with pillar height as a result of the increase in pinning and the contact line friction associated with an increased sidewall area. The losses are also expected to be inversely proportional to the void space between the pillars because a larger void space reduces the viscous shear associated with fluid recession. Parameter $b - a$ is a measure of the void space. Combining the two mechanisms of energy loss, we expect the energy losses to be proportional to $h/(b - a)$. The frictional force parameter c_f is obtained as

$$c_f = \frac{e_{lost}}{h/(b-a)} \quad (7)$$

The last two columns in Table 1 list the values of e_{lost} and c_f. We conclude from experiments on surface 1 that e_{lost} does not depend on the magnitude of the wetting voltage. The energy lost per unit sidewall area e_{lost} is seen to be proportional to parameter $h/(b - a)$, and c_f is approximately 60 mJ/m^2. This verifies our hypothesis that shorter pillars with increased pitch offer reduced frictional forces that impede the reverse transition. The energy losses as calculated in Table 1 are seen to be similar in magnitude to the surface energy density of water, which is 72 mJ/m^2. This comparison clearly illustrates that nonconservative frictional forces strongly influence the fluid behavior in the Wenzel state.

In summary, we introduced the concept of achieving the dewetting Wenzel−Cassie transition using an opposing electric field. We experimentally demonstrated this approach to be a reliable and repeatable tool for achieving dewetting without mass loss; this technique thus has important advantages over other schemes that have been proposed for reversing the wetting transition. This reversible transition technique can be utilized, for example, in lab-on-a-chip applications for analyzing biological specimens that cannot be subjected to boiling,[14] vibration,[20] or an ambient oil environment.[16,17] We numerically estimated the strength of various dissipative forces through careful experimentation and established the influence of surface structure on the frictional forces. Numerous previous studies have reported the "stickiness" of Wenzel-state droplets; our work quantifies these forces. Additional studies are needed to understand the nature of these forces fully; the present work offers important guidelines to minimize the influence of frictional forces in the Wenzel state.

■ ASSOCIATED CONTENT

Supporting Information. A movie showing multiple cycles of reversible transition (experiment corresponding to Figure 4), a discussion of the minimum droplet volume required for the successful reversible transition for the given plate height with some experimental results, and the droplet shapes from the droplet lift-off experiment to identify $V_{2\text{-crit}}$. This material is available free of charge via the Internet at http://pubs.acs.org.

■ AUTHOR INFORMATION

Corresponding Author

*E-mail: sureshg@purdue.edu. Tel: (765) 494 5621.

■ REFERENCES

(1) Cassie, A. B. D. *Discuss. Faraday Soc.* **1948**, *3*, 11–15.
(2) Wenzel, T. N. *J. Phys. Colloid Chem.* **1949**, *3*, 1466–1467.
(3) He, B.; Patankar, N. A.; Lee, J. *Langmuir* **2003**, *19*, 4999–5003.
(4) Mugele, F.; Baret, J. C. *J. Phys.: Condens. Matter* **2005**, *17*, R705–R774.
(5) Pollack, M. G.; Shenderov, A. D.; Fair, R. B. *Lab Chip* **2002**, *2*, 96–101.
(6) Baret, J.-C.; Brinkmann, M. *Phys. Rev. Lett.* **2006**, *96*, 146106.
(7) Kuo, J. S.; Spicar-Mihalic, P.; Rodriguez, I.; Chiu, D. T. *Langmuir* **2003**, *19*, 250–255.
(8) Monroe, C. W.; Daikhin, L. I.; Urbakh, M.; Kornyshev, A. A. *Phys. Rev. Lett.* **2006**, *97*, 136102.
(9) Kumari, N.; Bahadur, V.; Garimella, S. V. *J. Micromech. Microeng.* **2008**, *18*, 085018.
(10) Kumari, N.; Bahadur, V.; Garimella, S. V. *J. Micromech. Microeng.* **2008**, *18*, 105015.
(11) Herberston, D. L.; Evans, C. R.; Shirtcliffe, N. J; McHale, G.; Newton, M. I. *Sens. Actuators, A* **2006**, *130*, 189–193.
(12) Bahadur, V.; Garimella, S. V. *Langmuir* **2007**, *23*, 4918–4924.
(13) Bahadur, V.; Garimella, S. V. *Langmuir* **2008**, *24*, 8338–8345.
(14) Krupenkin, T. N.; Taylor, J. A.; Wang, E. N.; Kolodner, P.; Hodes, M.; Salamon, T. R. *Langmuir* **2007**, *23*, 9128–9133.

(15) Wang, Z.; Ci, L.; Chen, L.; Nayak, S.; Ajayan, P. M.; Koratkar, N. *Nano Lett.* **2007**, *7*, 697–702.
(16) Dhindsa, M.; Smith, N. R.; Heikenfeld, J.; Rack, P. D.; Fowlkes, J. D.; Doktycz, M. J.; Melechko, A. V.; Simpson, M. L. *Langmuir* **2006**, *22*, 9030–9034.
(17) Verplanck, N.; Galopin, E.; Camart, J.-C.; Thomy, V.; Coffinier, Y.; Boukherroub, R. *Nano Lett.* **2007**, *7*, 813–817.
(18) Heikenfeld, J.; Dhindsa, M. *J. Adhes. Sci. Technol.* **2008**, *22*, 319–334.
(19) Bahadur, V.; Garimella, S. V. *Int. J. Micro-Nano Scale Trans.* **2010**, *1*, 1–26.
(20) Boreyko, J. B.; Chen, C. -H. *Phys. Rev. Lett.* **2009**, *103*, 174502.
(21) Vrancken, R. J.; Kusumaatmaja, H.; Hermans, K.; Prenen, A. M.; Pierre-Louis, O.; Bastiaansen, C. W. M.; Broer, D. J. *Langmuir* **2010**, *26*, 3335–3341.
(22) Manukyan, G.; Oh, J. M.; Ende, D.; Lammertink, R. G. H.; Mugele, F. *Phys. Rev. Lett.* **2011**, *106*, 014501.
(23) Lapierre, F.; Brunet, P.; Coffinier, Y.; Thomy, V.; Blossey, R.; Boukherroub, R. *Faraday Discuss.* **2010**, *146*, 125–139.
(24) Lee, C.; Kim, C.-J. *Phys. Rev. Lett.* **2011**, *106*, 014502.
(25) See Supporting Information.